IEEE Access
Multidisciplinary ⋮ Rapid Review ⋮ Open Access Journal

Received 10 December 2023, accepted 23 January 2024, date of publication 13 February 2024, date of current version 27 February 2024.

Digital Object Identifier 10.1109/ACCESS.2024.3365551

RESEARCH ARTICLE

Unsupervised Feature-Preserving CycleGAN for Fault Diagnosis of Rolling Bearings Using Unbalanced Infrared Thermal Imaging Sample

LUJIALE GUO[1], JOON HUANG CHUAH[1,2], (Senior Member, IEEE), WONG JEE KEEN RAYMOND[1], XIAOHUI GU[3], JIE YAO[3], AND XIANGQIAN CHANG[3]

[1]Department of Electrical Engineering, Faculty of Engineering, Universiti Malaya, Kuala Lumpur 50603, Malaysia
[2]Faculty of Engineering and Information Technology, Southern University College, Skudai, Johor 81300, Malaysia
[3]State Key Laboratory of Mechanical Behavior and System Safety of Traffic Engineering Structures, Shijiazhuang Tiedao University, Shijiazhuang 050043, China

Corresponding author: Joon Huang Chuah (jhchuah@um.edu.my; jhchuah@sc.edu.my)

ABSTRACT The fault diagnosis of rolling bearing is of great significance in industrial safety. The method of infrared thermal image combined with neural network can diagnose the fault of rolling bearing in a non-contact manner, however its data in different scenes are often unbalanced and difficult to obtain. The generative adversarial networks can solve this problem by generating data with the required features. In this paper, an unsupervised learning framework named Feature-Preserving Cycle-Consistent Generative Adversarial Networks (FP-CycleGAN) is designed for defect detection in unbalanced rolling bearing infrared thermography sample. Since the classical Cycle-Consistent Generative Adversarial Networks (CycleGAN) often must balance the weights between generation, discrimination and consistency loss when doing the feature conversion from source domain to target domain, and the process often results in pattern collapse or feature loss. To avoid this problem, a new discriminator is designed to identify whether the generated image A and B belong to two different classes, and a new class loss are proposed. In order to better extract fault features and perform features migration, the new generator is reconstructed based on the U-Network structure, the convtraspose method of the up-sampling network is replaced by Bicubic Interpolation to effectively avoid the checkerboard effect of the generated images. The defect detection of the expanded dataset was performed using Residual Network and compared with the pre-expansion data to demonstrate the usability of the generated data and the superiority of the proposed FP-CycleGAN method for rolling bearing defect detection in small sample of infrared thermal images.

INDEX TERMS Fault diagnosis, rolling bearing, infrared thermal imaging, unbalanced data, generative adversarial networks.

I. INTRODUCTION

Currently, machinery plays a crucial role in various fields, and the rolling bearing system, as its core component, has always been a matter of great concern in terms of safety. In complex or high intensity working environments, bearings often suffer from damage such as corrosion, cracks, or spalling in the inner ring, outer ring, or rolling elements, which can potentially lead to industrial accidents.

Therefore, conducting fault detection on rolling bearings to proactively identify the damage and enhance system safety is important [1], [2], [3].

Vibration signals are frequently utilized as a method for diagnosing faults in bearings because bearings with different types of damage respond correspondingly to external stimuli while in operation, thus generating corresponding vibration fault signals within the vibration signal [4], [5]. However,

The associate editor coordinating the review of this manuscript and approving it for publication was Senthil Kumar.

vibration signal analysis faces several limitations, such as difficulties in sensor installation, the potential impact on equipment structure during signal acquisition, the variability of working conditions, and the presence of strong noise in practical application [6].

Recently, the combination of infrared thermal imaging and artificial intelligence has gained increasing attention in the non-destructive fault diagnosis of rotating machinery. Compared to vibration signals, infrared thermal imaging offers advantages such as easy installation, non-contact usage, and high precision [7]. Choudhary et al. proposed a method for detecting bearing defects using infrared thermal imaging by combining artificial neural networks with convolutional neural networks. Their approach addresses the challenge of early bearing failure detection under different bearing conditions [8]. Zhiyi et al. proposed a framework that combines a convolutional autoencoder with an enhanced convolutional neural network to achieve high diagnostic accuracy of small-labeled infrared thermal images for rotor bearings [9]. Most of the past data-driven defect detection methods are based on the premise that the training data samples are large, average, and easily available. However, in practical engineering applications, many defect samples under different conditions are very difficult to obtain, and deep learning models trained from samples in the laboratory usually do not work very well in practical engineering applications.

In industrial defect detection, it is often difficult to obtain the same amount of fault samples as healthy samples and the same characteristics as in real engineering, which leads to unsatisfactory results when the trained system is applied to complex conditions [10]. Many solutions have been proposed for this problem [11], [12]. Yu et al. proposed a cross-domain bearing diagnosis framework based on transferable features and watershed embedding discriminative distribution adaptation to compensate for the imbalance between two real rolling bearing datasets [13]. Zhu et al. designed a migration learning method based on the Maximum Mean Difference Multi-Kernel variant (MK-MMD), enabling pseudo label learning to resist data imbalance and improve prediction accuracy [14]. Ma et al. proposed two multi-label learning algorithms, personalized binary relevance (PBR) and hierarchical multi-label K-nearest neighbor (HML-KNN), for prognosis and health management (PHM) of rolling bearings, which exhibit fast modeling and high global information analysis capability in bearing fault analysis, respectively [15]. However, most of the solutions for imbalanced data based on transfer learning or label learning are unable to explore the deeper differences between different features and have limited effects. In contrast, generative networks based on deep learning have the advantage of extending sample diversity and can amplify data in an unsupervised or semi-supervised mode [16].

Classical generative models include Variational Autoencoders (VAEs) [17] and Generative Adversarial Networks (GANs) [18], which typically generate data of higher complexity and closer to the true distribution than VAEs [19]. GAN consists of two networks, a generator, and a discriminator, which can cleverly compute the difference between the distribution of the generated data and the distribution of the original data, so that the generated data can learn the features of the original data. Since the creation of GAN, various variants of GAN have emerged. Mirza and Osindero proposed CGAN, which generates type-specific data by adding a conditional vector to the input noise vector [20]. The goal of GAN training is to find the Nash equilibrium between the generator and the discriminator, but traditional GANs are often unstable and prone to pattern collapse due to the large oscillations between the generator and the discriminator during adversarial training. Moreover, the generator often generates a single output or non-ideal output to fool the discriminator, resulting in training failure. Radford et al. proposed DCGAN, which introduces convolutional neural networks to build generators and discriminators that can extract deeper features and generate higher quality images [21]. To solve the problem that when using JS Divergence, the value of JS Divergence for two distributions without overlapping is always Log2, and it is impossible to calculate the relationship between the two distributions in this state, Arjovsky et al. introduced the Wasserstein GAN. The Wasserstein distance was introduced on top of the traditional GAN to replace the original KL divergence and JS divergence. The Wasserstein divergence is used to calculate the distance between the original distribution and the generated distribution by using the idea of minimizing the earth mover's distance, which makes the GAN more stable and can generate higher quality data [22]. Later, in response to the problem that supervised learning algorithms require a large amount of data from two distributions corresponding to each other, but the data in the situation are often unbalanced, Zhu et al. proposed a model called CycleGAN, which transforms the features in the domain of two different distributions by constructing two sets of generators and discriminators, and introduced a loss function called ''cycle consistency loss'' which separates the key features from the rest of the data and fixes one to enable the other to be transformed. This enables the style migration of images. Probably the best-known example is their unsupervised training and image transformation on two image datasets of horses and zebras [23].

Recently, GAN has been gradually applied to solve the problem of engineering fault imbalance data. For example, Zhou et al. combined autoencoder (AE) and GAN to generate fault features for several different fault samples to improve the accuracy of fault diagnosis [24]. Chen et al. proposed a Joint Atrium and Scar Segmentations generative adversarial network (JAS-GAN) to segment unbalanced atrial targets from late gadolinium-enhanced cardiac magnetic resonance (LGE CMR) images in an end-to-end mode, producing better segmentation performance [25]. For health monitoring of civil structures, Luleci et al. proposed a deep convolutional

GAN incorporating Wasserstein loss (CycleWDCGAN-GP), which allows the undamaged and damaged acceleration data to be transformed between the two domains and can be used for the possible response of healthy structures to potentially damaged conditions, solving the problem of scarcity and imbalance of SHM data [26].

However, datasets generated using GAN often suffer from the problem of lack of realism and usability, and it is challenging to generate data with a natural distribution of fault features. There is still a lack of research on imbalanced data from infrared thermal images of bearings, and Cyclegan can transform features and generate images between thermal images of bearings with different types of faults, while maintaining the natural distribution of the images. However, further research and experimental validation is needed for how to generate high quality images using generative loss, adversarial loss, cycle consistency loss and identity loss to preserve and migrate target and non-target features in both domains while avoiding pattern collapse and gradient disappearance.

In summary, this paper proposes a fault diagnosis framework called Feature Preserving CycleGAN. The core of the framework is the introduction of a new discriminator D_AB based on CycleGAN to constrain the non-target features in the source domain, which in turn migrates the target features in the source domain and reconstructs the generator structure. It solves the problem of data imbalance in the infrared thermal images of faulty rotor bearings and enhances the stability of the network and the realism of the generated images during the adversarial generation process. The main contributions of this paper are as follows:

- A new unsupervised fault diagnosis method called FP-CycleGAN is proposed. A new discriminator D_AB is introduced to efficiently migrate the target features while maintaining the non-target features during the transformation of the bearing thermal image from the source domain A to the target domain B. The total Loss function is reconstructed, and a new Loss-class is added.
- The generator is reconstructed to provide better feature extraction capability and data processing speed. It is possible to reduce the higher data volume caused by D_AB and the difficulty of bearing thermal image reconstruction in the new framework, which improves the operation speed of the network and the quality of the generated images.
- Using the rotor bearing infrared thermal image fault simulation experiment bench to extract data and conduct extensive experiments, to verify the effectiveness of the proposed data amplification and fault diagnosis method.

The rest of the paper is designed as follows: In Section II the theoretical background is briefly described. In Section III the implementation of the proposed method is described in detail. In Section IV, the data collection method is introduced and the results of the experimental analysis of the rotor bearing thermal images for fault detection are presented. Finally, a summary is presented in Section 5.

II. RELATE WORKS

The use of GANs for meaningful feature migration is a challenging problem that has attracted much interest. In this section, we provide some existing methods for improving the quality of feature migration and image generation. Depending on the functionality of the methods, they can be classified as adversarial training, image reconstruction, and computational difficulty reduction.

A. GENERATIVE ADVERSARIAL NETWORKS

The basic structure of GAN is shown in Figure 1, where x represents the real sample and obeys the prior distribution of P_r. z represents the random noise of the input into the network and obeys the prior distribution of P_z. Generally, P_z often uses Gaussian distribution and Uniform distribution. G represent the Generator, and the input z can be mapped into a fake sample $G(z)$ and obeys the distribution P_g. Then $G(z)$ and x will be input discriminator (D) to judge whether they conform to the prior distribution P_r, to achieve direct confrontation between G and D and achieve Nash equilibrium by constantly adjusting parameters.

The objective function of GAN is:

$$\min_G \max_D L(G, D) = E_{x\sim P_r}[logD(x)] + E_{z\sim P_z}[log(1 - D(G(z)))] \quad (1)$$

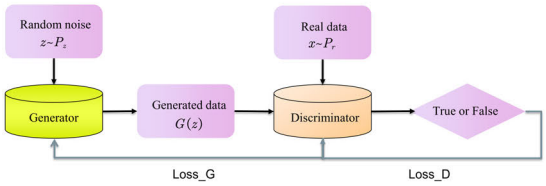

FIGURE 1. Basic structure of GAN.

Here, the loss of G is $\log(1 - D(G(z)))$, and the loss of D is $-(\log(D(x))) + \log(1 - D(G(z)))$. G hopes that the generated data deceives D, that is, $D(G(z))$ is close to 1. D hopes to detect the data generated by G, that is, $D(G(z))$ is close to 0, so that they can realize adversarial training and make P_g as close as possible to P_r, that is, the generated samples conform to the real sample distribution as much as possible [20].

B. CYCLE CONSISTENT GENERATIVE ADVERSARIAL NETWORK

In the field of image processing, the main purpose of CycleGAN is to exchange features between two images of different domains. It contains two generators, G_AB and G_BA, which can convert image A to B and image B to A respectively. It also contains two discriminators, D_A and D_B, which determine the authenticity of the generated and original images. The basic structure is shown in Figure 2.

The core idea is that we want Real A to have not only the target features of the sample B distribution, but also the

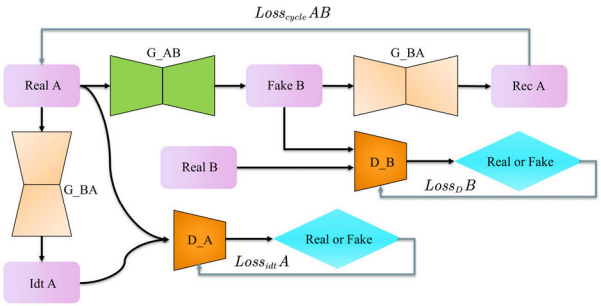

FIGURE 2. Basic structure of CycleGAN.

non-target features of the A distribution except for the target features, after Real A has been transformed into Fake B by G_{AB}. To achieve this, Cycle Consistency Loss and Identity Loss are introduced.

Cycle Consistency Loss is achieved by feeding Fake B back into generator G_{BA}, producing an image Rec A that is as similar as possible to the original Real A, which can be described as:

$$G_{BA}\left(G_{AB}(A)\right) = A \tag{2}$$

However, it is difficult to keep the non-target features unchanged only by Cycle Consistency Loss, because G_{AB} may learn the non-target features of non-input Real A, and the universal non-target features from other real pictures in the source domain can deceiving D_A as well. To solve this problem, Identity Loss is introduced.

Identity Loss is realized by directly inputting Real A into generator G_{BA} to generate picture Idt A, and constraining Idt A to have only the characteristics of the input picture Real A, without mixing the characteristics of other pictures from the source domain, which can be expressed as:

$$G_{BA}(A) = A \tag{3}$$

When training the discriminator, the parameters of G_{AB} and G_{BA} will be fixed and only the parameters of D_A and D_B will be adjustable, and the target will be changed from Minimize Loss to Maximize Loss.

C. INTERPOLATION ALGORITHM

In the past, it was found that the up-sampling process of GAN for image generation often uses transpose convolution for image reconstruction, but this often leads to a tessellation effect (uneven overlap) in the generated images. The cause of this phenomenon is often considered to be frequency artifacts since the kernel size of the convolution is not divisible by the stride [27]. This problem can be effectively avoided by using interpolation methods, such as nearest neighbor interpolation, bilinear interpolation and bicubic interpolation, of which bicubic interpolation is more computationally intensive but has the best results.

The bicubic interpolation uses the values of the 16 points around the point to be sampled to interpolate three times, considering the rate of change of the values of each neighboring point in addition to the directly adjacent points. The formula is:

$$B\left(X, Y\right) = \sum_{i=0}^{3}\sum_{j=0}^{3} a_{ij} \times W(i) \times W(j) \tag{4}$$

where $B\left(X, Y\right)$ is the target pixel, i and j are the rows and columns of the points to be sampled, and $W(x)$ is the Bicubic function:

$$W(x) = \begin{cases} (a+2)\,|x|^3 - (a+3)\,|x|^2 + 1 & for\ |x| \leqslant 1 \\ a|x|^3 - 5a|x|^2 + 8a\,|x| - 4a & for\ 1 < |x| < 2 \\ 0 & otherwise \end{cases} \tag{5}$$

where a is the weight, often taken as -0.5.

D. DEPTHWISE SEPARABLE CONVOLUTION

Depthwise Separable Convolution is a form of convolution with factorization and is probably best known for its application in Mobile Nets, proposed by Howard et al. in 2017. Compared to traditional 3D convolution, Depthwise Separable Convolution reduces computational effort by splitting the standard convolution into two steps: depth convolution and point convolution [28].

The computation number C and the parametric number P of the standard 3D Convolution are:

$$C = D_k \times D_k \times M \times N \times D_F \times D_F \tag{6}$$

$$P = D_k \times D_k \times M \times N \tag{7}$$

where D_F×D_F×M is input feature maps, D_K×D_K×M is kernel size, D_F×D_F×N is output feature maps.

The computation C_{DS} and the parametric number P_{DS} of the Depthwise Separable Convolution are:

$$\begin{aligned} C_{DS} &= C_{depth} + C_{point} \\ &= D_k \times D_k \times M \times D_F \times D_F + M \times N \times D_F \times D_F \end{aligned} \tag{8}$$

$$P_{DS} = P_{depth} + P_{point} = D_k \times D_k \times M + M \times N \tag{9}$$

where C_{depth} and P_{depth} is the computation and parametric number respectively.

Computational volume analysis of standard convolution with depthwise separable convolution:

$$\begin{aligned} \frac{C_{DS}}{C} &= \frac{D_k \times D_k \times M \times D_F \times D_F + M \times N \times D_F \times D_F}{D_k \times D_k \times M \times N \times D_F \times D_F} \\ &= \frac{1}{N} + \frac{1}{D_K^2} \end{aligned} \tag{10}$$

This shows that with a 3×3 convolutional kernel, the parameters can be reduced by a factor of 8 to 9 with almost no loss of accuracy.

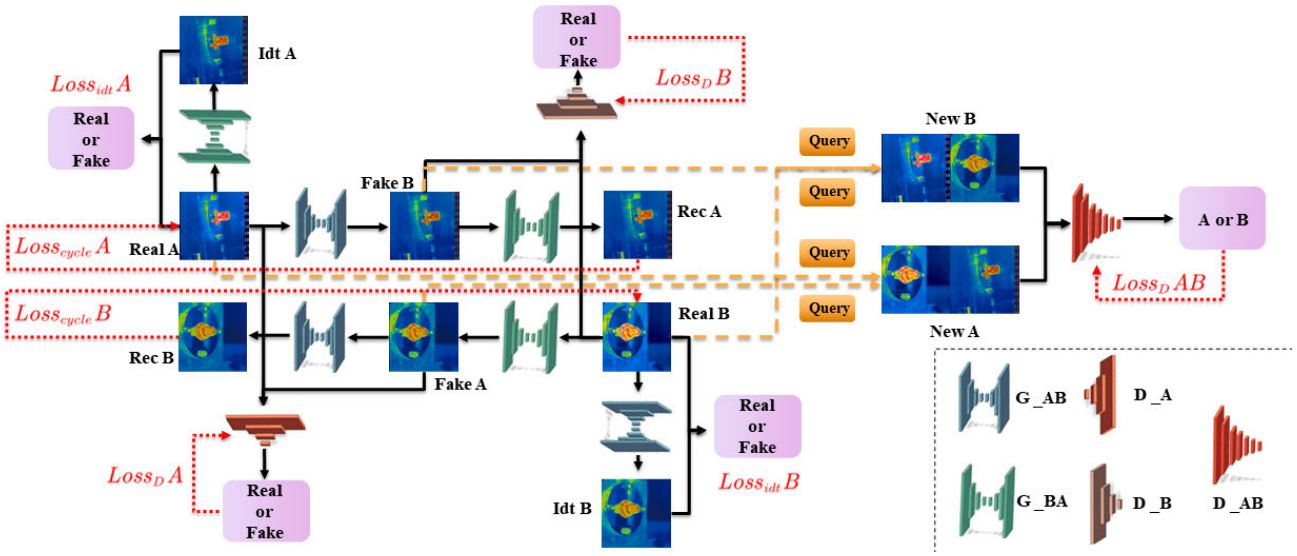

FIGURE 3. The framework of the FP-Cyclegan.

III. PROPOSED FRAMEWORK

The framework of the proposed unsupervised rotor bearing unbalance fault diagnosis method is shown in Figure 3.

The main steps are as follows:

Step 1: For the network main process, the real images Real A and Real B enter the generators G_AB and G_BA respectively to generate the target dummy images Fake B and Fake A. The generated The generated images then enter the generators G_BA and G_AB to generate the reconstructed images Rec A and Rec B.

Step 2: For the input of the new discriminator D_AB, each generated fake image and the corresponding real image are extracted into the image buffer with Query probability (total probability 1). Real A and Fake A compose the image buffer A, from which a random image is extracted and named New A. New B is generated by the same process.

Step 3: For the loss function, Real A is compared with Fake A by means of the discriminator D_A and the loss value is calculated using BCE. The process for Image B is the same as for A. In addition, New A and New B enter the discriminator D_AB for binary classification, and the loss value is calculated using the cross-entropy function.

Step 4: Sum all the Losses for gradient feedback and network parameter update, and finally the trained network is used to amplify the data and calculate the final accuracy and other metrics.

A. ARCHITECTURE OF THE GENERATOR

With the development of Transformer frameworks based on self-attentive mechanisms, excellent vision backbone frameworks such as Vision Transformers (ViTs), Swin Transformers, etc. have emerged in the field of recognition vision and seem to be gradually replacing the old ConvNets [29], [30].

However, Z. Liu et al. found that, with the same key components of the network, ConvNets still have advantages that cannot be replaced by the self-attentive mechanism and re-examined the design space to propose a network framework called ConvNeXt to achieve results comparable to those of Transformer [31]. Inspired by ConvNeXt, we designed a U-shaped network based on the ConvNeXt module for the generators of Cyclegan networks.

The architecture of the ConvNeXt Block is shown in Figure 4.

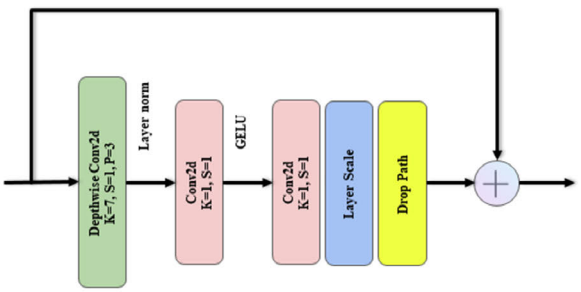

FIGURE 4. The architecture of the ConvNeXt block.

The input is first passed through a depthwise separable convolutional layer with the kernel size of 7, the step size of 2, and the padding of 3, and then through two 1×1 convolutional layers. Before the output, a scaling factor called layer scale is applied to adjust the expressiveness of the layer output and a drop path is introduced to randomly discard network paths to prevent overfitting and improve generalization.

The architecture of the generator is shown in Figure 5.

First, the pre-processing process scales and center crops the bearing thermal image to the size of $224 \times 224 \times 3$ as input.

For the down-sampling process, the image is first projected into a $56 \times 56 \times 96$ feature map by a convolutional layer with a kernel size and stride of 4. The feature map is then down sampled three times, with each down sample module consisting of multiple ConvNeXt Blocks and a Conv2d layer.

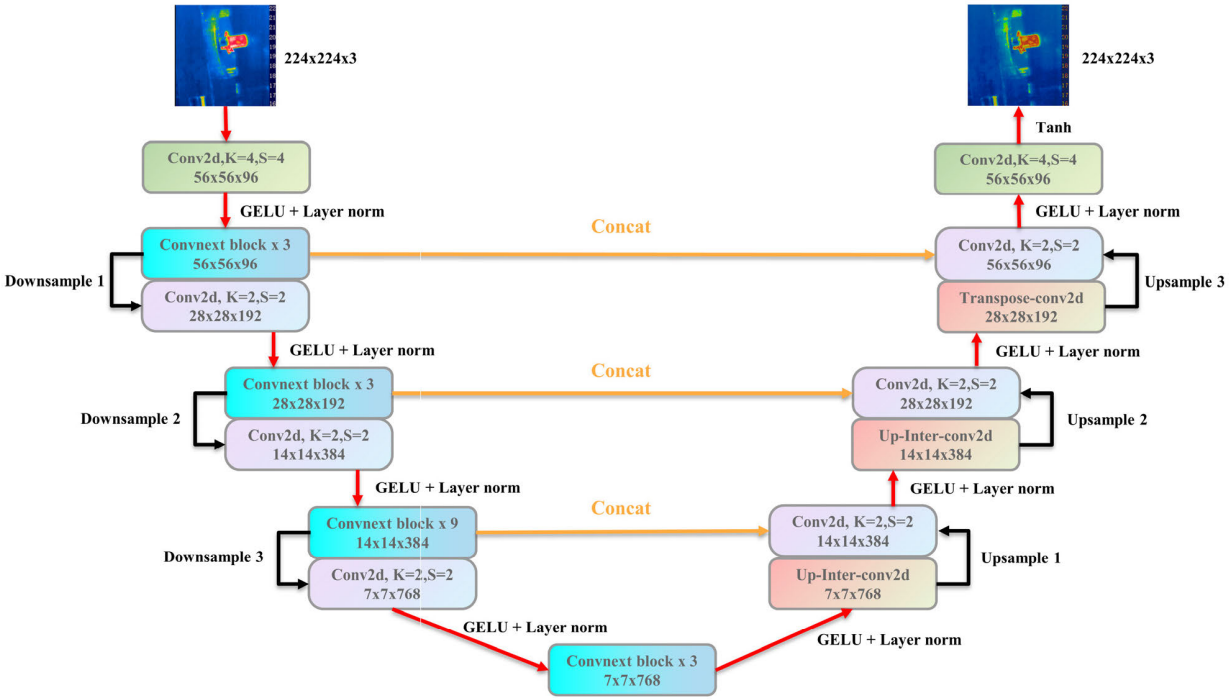

FIGURE 5. The architecture of the generator.

The final feature map of size $7 \times 7 \times 768$ enters a bottleneck layer consisting of three ConvNeXt Blocks. We keep the same number of blocks as in ConvNeXt-T [3,3,9,3].

For the up-sampling process, the output of the bottleneck layer is passed through three up sample modules, each consisting of a linear Interpolation or Transpose Covn2d layer and a Conv2d layer. We also introduce Network Layer Fusion, which concat the corresponding feature map sizes from the down-sampling and up-sampling processes in the channel dimension to improve the expressiveness of the model and the perception of different levels of features in the image. The final feature map is reconstructed back to an input size of $224 \times 224 \times 3$ by a Transpose Covn2d layer with the kernel size and step size of 4 and output by Tanh as the activation function.

Throughout the generator process, we used a smoother GELU and a more feature focused Layernorm as the activation function and normalization method after each layer of the network to improve the model's generalizability and training speed.

B. ARCHITECTURE OF THE GENERATOR

The structure of the new discriminator D_AB is shown in Figure 6.

The input to D_AB is the same as D_A and D_B, both being pre-processed $224 \times 224 \times 3$ images of the centre of the rotor bearing thermal image. The difference is that the new D_AB finally compresses the feature map to $1 \times 1 \times 3072$ and outputs it as a $4 \times 1 \times 1 \times 2$ matrix with a fully-connected layer, where 4 is the batch size and 2 is the target score for binary classification. The reason for this is to use CrossEntropyLoss instead of MSELoss to avoid the problem of non-decreasing gradients when the output is close to 0 or 1.

C. ARCHITECTURE OF THE GENERATOR

The loss function of the whole model is:

$$Loss_{FP-Cyclegan} = Loss_{gan} + Loss_{cycle} + \lambda Loss_{idt} + Loss_{class} \tag{11}$$

where $Loss_{gan}$ is the classical GAN network adversarial loss, for the FP-Cyclegan network there are two generators and two discriminators, so its expression is:

$$\begin{aligned} Loss_{gan} &= \mathcal{L}_{gan}\left(G_{AB}, D_B, A, B\right) + \mathcal{L}_{gan}\left(G_{BA}, D_A, A, B\right) \\ &= \mathbb{E}_{a\sim P_{data}(a)}\left[\log D_A(a)\right] \\ &\quad + \mathbb{E}_{b\sim P_{data}(b)}\left[log\left(1 - D_A\left(G_{BA}(b)\right)\right)\right] \\ &\quad + \mathbb{E}_{b\sim P_{data}(b)}\left[log D_B(b)\right] \\ &\quad + \mathbb{E}_{a\sim P_{data}(a)}\left[log\left(1 - D_B\left(G_{AB}(a)\right)\right)\right] \end{aligned} \tag{12}$$

The goal of the generator is to bring the defective features of the generated image closer to the distribution of defective features in the target domain, and the goal of the discriminator is to be able to identify whether the image contains defective features in the source domain or in the target domain.

Expression of the optimization objective in a mathematical formula:

$$G_{AB}^*, G_{BA}^*, D_A^*, D_B^* = arg \min_{G_{AB}^*, G_{BA}^*} \max_{D_A, D_B} \mathcal{L}\left(G_{AB}, G_{BA}, D_A, D_B\right) \tag{13}$$

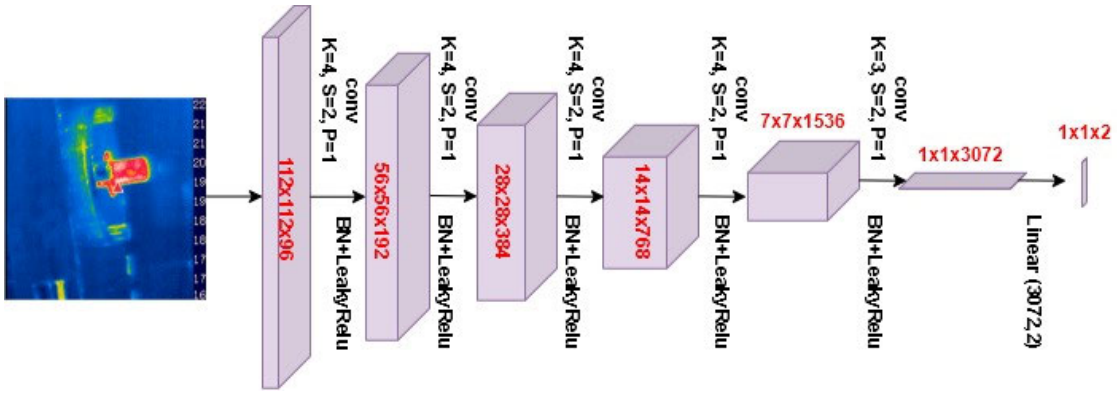

FIGURE 6. The architecture of the discriminator D_AB.

In addition, we used MES Loss to calculate the loss of both, and set the generated image label to 0 and the original image label to 1. The mathematical formula is:

$$\min_{D_B} \frac{1}{N} \sum_{i=1}^{N} MSE\left(D_B(b), 1\right) \tag{14}$$

$$\min_{D_A} \frac{1}{N} \sum_{i=1}^{N} MSE\left(D_A(a), 1\right) \tag{15}$$

$$\min_{G_{AB}} \frac{1}{N} \sum_{i=1}^{N} MSE\left(D_B\left(G_{AB}(a)\right), 0\right) \tag{16}$$

$$\min_{G_{BA}} \frac{1}{N} \sum_{i=1}^{N} MSE\left(D_A\left(G_{BA}(b)\right), 0\right) \tag{17}$$

The expression for $Loss_{cycle}$ is:

$$\begin{aligned} Loss_{cycle} = {} & \mathbb{E}_{a\sim P_{data}(a)}\left[\|G_{BA}\left(G_{AB}(a)\right) - a\|\right] \\ & + \mathbb{E}_{b\sim P_{data}(b)}\left[\|G_{AB}\left(G_{BA}(b)\right) - b\|\right] \end{aligned} \tag{18}$$

$Loss_{cycle}$ is implemented as L1 Loss, which, when minimizing $Loss_{cycle}$, is equivalent to making the input image as consistent as possible with the image reconstructed by the two generators. This enables the generated image to acquire the fault features in the target domain while keeping the other non-target features in the source domain as constant as possible.

The expression for $Loss_{idt}$ is:

$$\begin{aligned} Loss_{idt} = {} & \mathbb{E}_{a\sim P_{data}(a)}\left[\|G_{BA}(a) - a\|\right] \\ & + \mathbb{E}_{b\sim P_{data}(b)}\left[\|G_{AB}(b) - b\|\right] \end{aligned} \tag{19}$$

$Loss_{idt}$ is implemented as L1 Loss, when minimizing $Loss_{idt}$, the generated images try to keep the non-target features of that original input image while obtaining the defective features of the target domain, instead of the non-target features of other images in the source domain.

The expression for $Loss_{class}$is:

$$\begin{aligned} Loss_{class} = {} & \mathcal{L}_{class}\left(G_{AB}, D_{AB}, A, B\right) + \mathcal{L}_{class}\left(G_{BA}, D_{AB}, A, B\right) \\ = {} & \mathbb{E}_{newa\sim P_{data}(newa)}\left[\log D_{AB}(newa)\right] \\ & + \mathbb{E}_{newb\sim P_{data}(newb)}\left[\log\left(1 - D_{AB}\left(G_{BA}(newb)\right)\right)\right] \\ & + \mathbb{E}_{newb\sim P_{data}(newb)}\left[\log D_{AB}(newb)\right] \\ & + \mathbb{E}_{newa\sim P_{data}(newa)}\left[\log\left(1 - D_{AB}\left(G_{AB}(newa)\right)\right)\right] \end{aligned} \tag{20}$$

where $P_{data}(newa)$ is the joint distribution of the original image A distribution and the generated image A distribution, and $P_{data}(newb)$ is the same.

$$\begin{aligned} P_{data}(newa) = {} & \mu P_{data}(a) + (1-\mu)\, P_{data}\left[G_{BA}(b)\right] \\ & b \sim P_{data}(b) \end{aligned} \tag{21}$$

$$\begin{aligned} P_{data}(newb) = {} & \mu P_{data}(b) + (1-\mu)\, P_{data}\left[G_{AB}(a)\right] \\ & a \sim P_{data}(a) \end{aligned} \tag{22}$$

where μ is the ratio of the original images to the generated images in the new joint distribution, used to control the degree of transfer of the target features.

In addition, $Loss_{class}$ is implemented as Cross Entropy Loss instead of MSE Loss because the objective of the new discriminator D_AB can be seen as a logistic regression problem to classify images from *newa* and *newa* as binary categories. MSE Loss is more suitable for linear regression problems.

In summary, if the features contained in the original input images A and B are represented by F_A and F_B. Use F_(G_BA (B)) and F_(G_AB (A)) to represent the features contained in the generated images Fake A and Fake B. with PF_A and PF_B representing the defective features of images A and B. with NF_A and NF_B representing the non-defective features of images A and B. Then the input image features are:

$$F_A = (PF_A, NF_A) \tag{23}$$

$$F_B = (PF_B, NF_B) \tag{24}$$

The goal of FP-Cyclegan's output image features is:

$$F_{G_{BA}(B)} = (PF_B, NF_A) \tag{25}$$

$$F_{G_{AB}(A)} = (PF_A, NF_B) \tag{26}$$

IV. EXPERIMENTAL VERIFICATION

A. COLLECTION AND DESCRIPTION OF LABORATORY BEARING DATA SETS

The faulty rotor bearing specimens used in the text are seven kinds of bearings with different failure points and degrees of damage, with a dimensional size of 650 mm outer ring radius and GCr15 material, and health condition names with corresponding labels as shown in Table 1.

The label N indicates damage to the inner ring, Q indicates damage to the sphere, W indicates damage to the outer ring and the number indicates the degree of damage.

The infrared thermal image acquisition process of this experiment was carried out at the State Key Laboratory of Mechanical Behaviour and System Safety of Traffic Engineering Structures, Shijiazhuang Tiedao University. The experimental data came from the rotating machinery test bench shown in Figure 7, mainly consisting of a driven motor, rotor shaft, bearing under test and drive belt. The infrared thermal imaging camera used is A315 made by FLIR, USA, which can collect the temperature field information of the faulty bearing at various points in the rotation, with a thermal sensitivity less than or equal to 0.05°C and a maximum acquisition temperature of 1200°C. The resolution was set to 370×240 pixels when shooting the camera is initially installed at 40cm from the fixed rotor shaft, and the position will change as the experiment progresses.

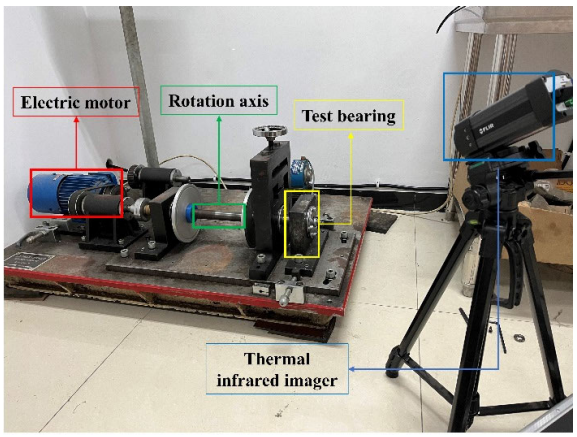

FIGURE 7. The rotating machinery test bench.

TABLE 1. Health conditions and labels of rolling bearings.

Health Condition	Amount (Multi dimension)	Amount (single dimension)	Label
F-N-0.6	300	400	Label 1
F-N-0.8	896+300	400	Label 2
F-N-1.0	300	400	Label 3
F-Q-0.8	300	400	Label 4
F-W-0.6	300	400	Label 5
F-W-0.8	300	400	Label 6
F-W-1.0	300	400	Label 7

The shooting software uses the professional analysis/detection system (BM_IR) of infrared thermal imager matched with A315. The interface is shown in Figure 8, the measuring range is -20.15-119.85, and the shooting frame rate is set to 1fps.

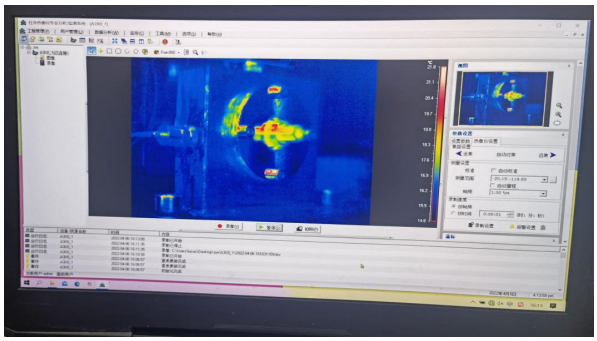

FIGURE 8. Thermal image acquisition system.

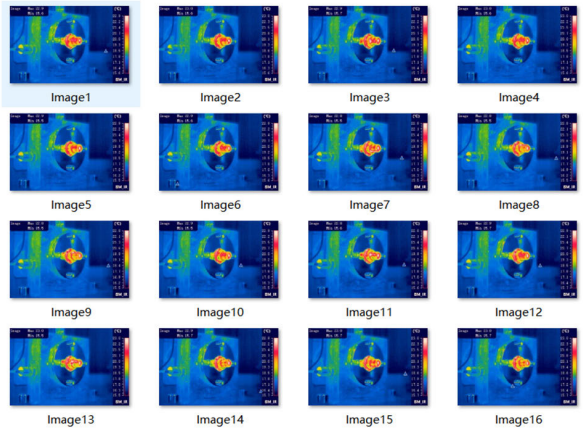

FIGURE 9. Single angle and state bearing rain900 data set.

In the first stage of the experiment, thermal imaging images were taken at five speeds (1,000, 2,000, 3,000, 4,000 and 5,000 rev/min) for each healthy condition of the bearing at a constant distance, and 80 images were taken for each speed condition, i.e., 400 experimental images for each bearing, for a total of 2,800 images. After the shooting, BTV files were obtained, and the files were transcoded to obtain a dataset of 2,800 images in the rain900 style, as shown in Figure 9.

400 images of each of the seven healthy conditions of the bearing at random speeds were acquired at random distances and angles between the thermal imaging camera and the faulty bearing. This was used to construct a test set to simulate the data diversity in a real application. It was also converted to the rain900 style as shown in Figure 10.

B. SAMPLE EXPANSION PERFORMANCE EVALUATION

The experimental algorithms in this paper were designed using Python 3.7.3 and Pytorch Stable (2.0.1). The experimental platform consists of an Intel Core i5-12400 CPU, NVIDIA RTX 3090 GPU and 32G RAM.

The hyperparameters of the FP-CycleGAN framework are set as shown in Table 2.

where Q (μ in formula 21/22) is the proportion of real images in the image buffer used for discriminator D_AB training,

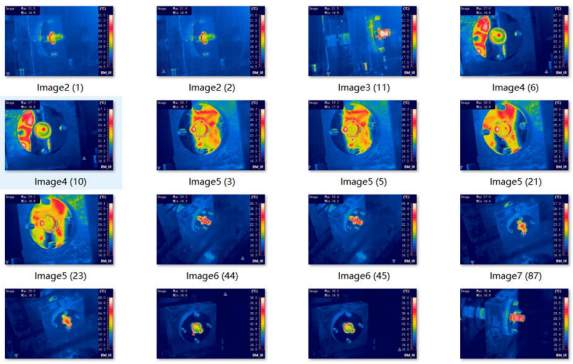

FIGURE 10. Single angle and state bearing rain900 data set.

TABLE 2. Hyperparameter setting.

Hyperparameter	Value
Adam Learning Rate	0.0001
Adam momentum term	0.5
Batch size	4
Number of epochs	300
Number of epochs with decay	300
Load image size	260
Crop image size	224
Q	0.9
λ	10

and λ is the weight of $Loss_{cycle}$. These hyperparameters were determined experimentally.

The experimental scheme for the sample expansion was to use 896 F-N-0.8 bearing thermal images with multi-state information as domain A, and 400 of one of the other six single-state bearing thermal images as domain B, converting them in turn. The aim is to transform the defective features of the thermal image of domain B with those of domain A to obtain the 896 generated multi-state images of domain B, thus enabling the expansion of the imbalance data.

To fully demonstrate the superiority of the proposed approach, it is necessary to investigate in turn the impact of the different modules of the FP-CycleGAN system on the system. A variety of evaluation metrics are used to quantify the different performances of the proposed model. The Fréchet Inception Distance (FID) value is a metric used to quantify the dissimilarity between images generated by a Generative Adversarial Network (GAN) and real images [32]. It measures the distance between the distributions of feature representations extracted from a pre-trained neural network, typically an Inception network. A lower FID score indicates that the generated images are closer to the real images in terms of their high-level features, implying better performance of the GAN in generating realistic images.

However, this metric can only be used to evaluate whether the generated images match the target domain distribution but cannot measure whether the migration of the target feature distribution can be performed while preserving to the maximum extent the non-target feature distribution in the source domain. So, in the experiment, it is necessary to strive for both lowering the FID value and improving the accuracy of the final classification network.

The time metric Time is used to evaluate the amount of data and the speed at which the model can be run.

Models with different up-sampling methods and convolution methods are combined with the proposed best models for comparison. All methods are tested in ten runs to overcome particularity and contingency.

All tables with an asterisk (*) represent the optimal approach in the proposed FP-CycleGAN framework.

Table 3 shows the operation time and FID values for the FP-CycleGAN with different up-sampling methods.

Figure 11 shows the images generated by the different up-sampling methods.

TABLE 3. Results of different up-sampling methods.

Up-simple method	Time (s/epoch)	FID score
Transposed Convolution	97.75	65.7604
Nearest neighbour interpolation (Step 1,2)	91.57	62.7155
Bilinear interpolation (Step 1,2)	98.14	62.5304
Bicubic interpolation* (Step 1,2)	**103.95**	**59.7446**
Bicubic interpolation (Step 1,2,3)	105.45	60.5247
Bicubic interpolation (Step 1,2,3,4)	120.50	85.0308
Bicubic interpolation (Step 3,4)	102.60	94.3045

The comparison shows that the interpolation algorithm can improve the quality of the images and avoid the tessellation effect as much as possible. Bicubic interpolation gives the best results for the generated images. The interpolation algorithm works better in the first half of the up-sampling (step1 and step2), whereas it reduces the quality of the resulting image in the latter half.

TABLE 4. Results of different convolution methods.

Up-simple method	Time (s/epoch)	FID score
Deep wise*	**103.95**	**59.7446**
Original	114.6	60.8022

Table 4 shows the operation time and FID values for different convolution methods. The results show that the computation time of the generator structure with depth wise separable convolution is significantly less than that with normal convolution.

C. UNBALANCE FAULT DIAGNOSIS RESULTS AND ANALYSIS

After determining the optimal FP-CycleGAN data augmentation framework, further comparative experiments for the diagnosis of thermal images of unbalanced faulty bearings are

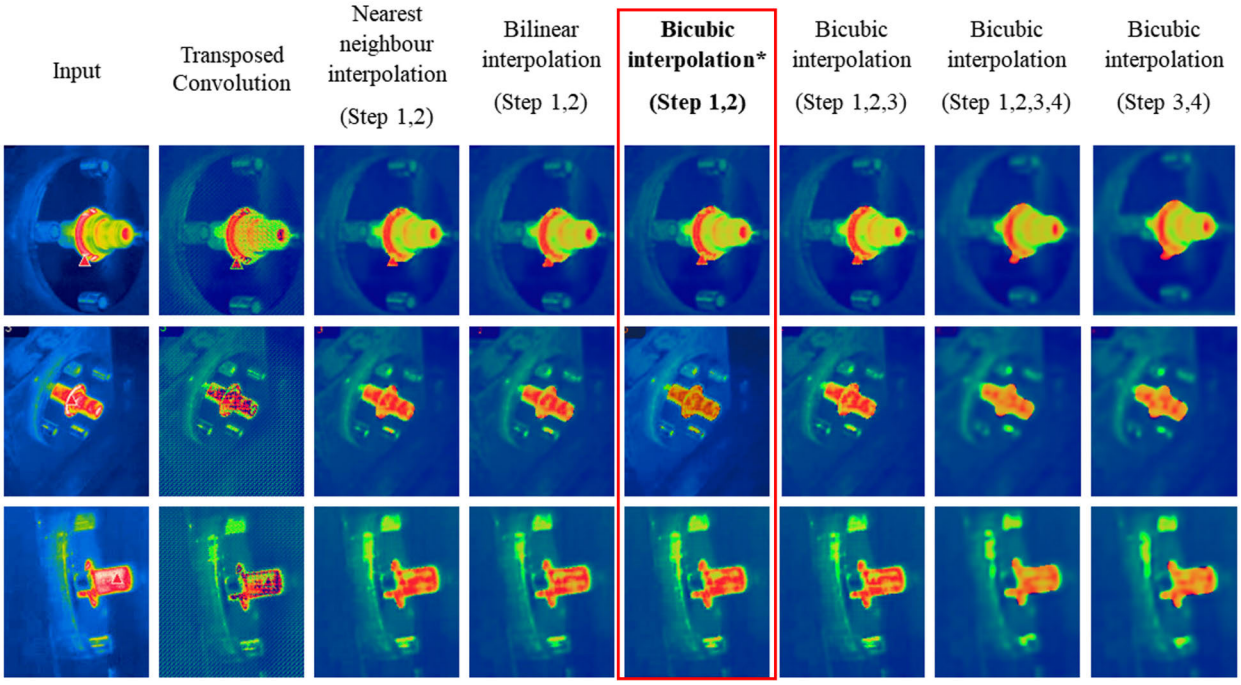

FIGURE 11. Images generated by different up-sampling methods.

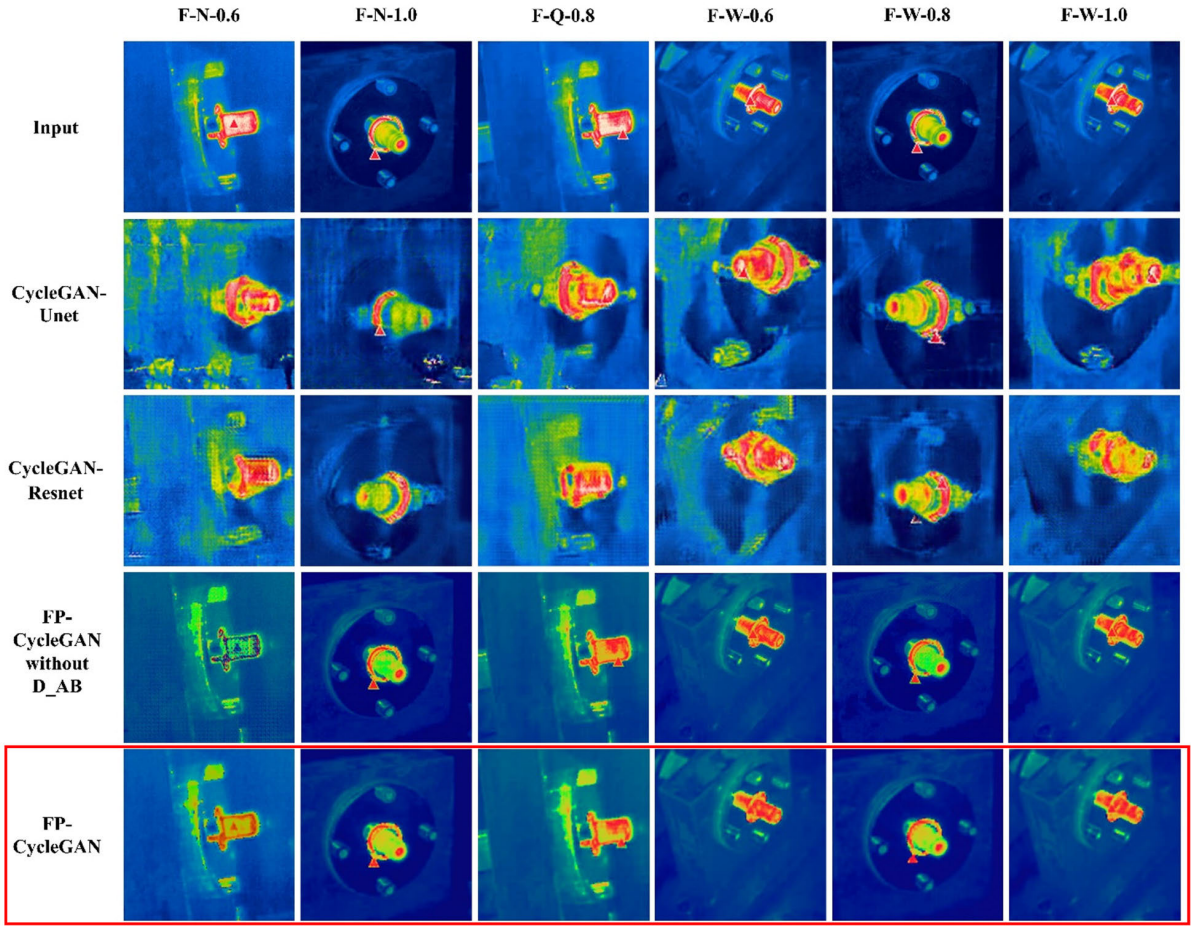

FIGURE 12. Images generated by different data amplification methods.

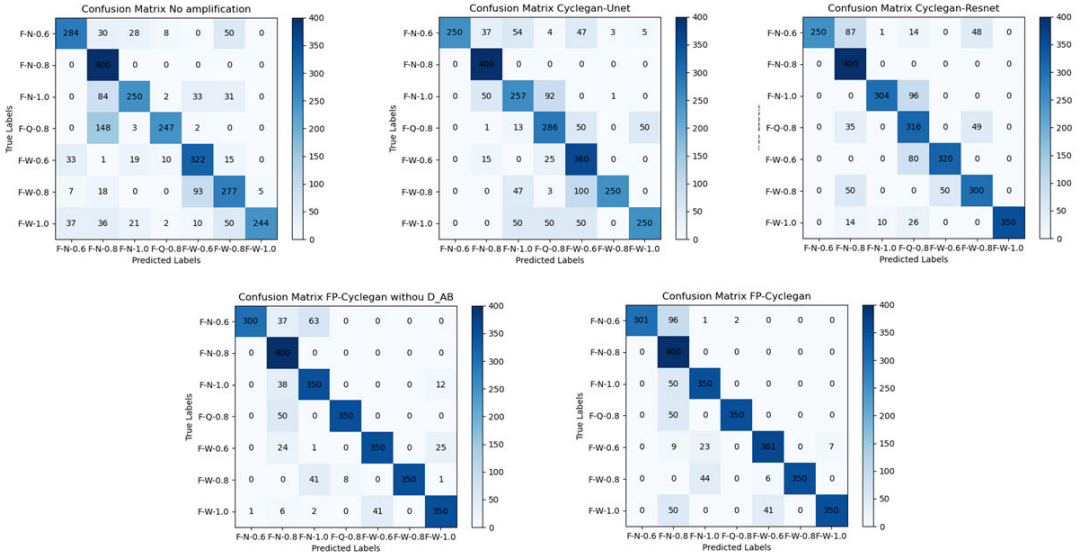

FIGURE 13. Confusion matrix for the classification network trained on the original and different data amplification datasets.

TABLE 5. Results of different data amplification method.

Data Amplification Method	Label	Pre (%)	Rec (%)	F1 (%)	Mean Pre (%)	Top-1 Acc (%)	Mean F1(%)
No Amplification	F-N-0.6	78.67	71.00	74.64	76.81	72.29	72.41
	F-N-0.8	55.79	100.00	71.62			
	F-N-1.0	77.88	62.50	69.35			
	F-Q-0.8	91.82	61.75	73.84			
	F-W-0.6	70.00	80.50	74.88			
	F-W-0.8	65.48	69.25	67.31			
	F-W-1.0	97.99	61.00	75.19			
CycleGAN-Unet	F-N-0.6	100.00	62.50	76.92	77.49	73.32	73.36
	F-N-0.8	79.52	100.00	88.59			
	F-N-1.0	61.05	64.25	62.61			
	F-Q-0.8	62.17	71.50	66.51			
	F-W-0.6	59.31	90.00	71.50			
	F-W-0.8	98.43	62.50	76.45			
	F-W-1.0	81.97	62.50	70.92			
CycleGAN-ResNet	F-N-0.6	100.00	62.50	76.92	83.75	80.00	80.38
	F-N-0.8	68.26	100.00	81.14			
	F-N-1.0	96.51	76.00	85.03			
	F-Q-0.8	59.40	79.00	67.81			
	F-W-0.6	86.49	80.00	83.12			
	F-W-0.8	75.57	75.00	75.28			
	F-W-1.0	100.00	87.50	93.33			
FP-CycleGAN without D_AB	F-N-0.6	99.67	75.00	85.59	89.40	87.50	87.72
	F-N-0.8	72.07	100.00	83.77			
	F-N-1.0	76.59	87.50	81.68			
	F-Q-0.8	97.77	87.50	92.35			
	F-W-0.6	89.51	87.50	88.50			
	F-W-0.8	100.00	87.50	93.33			
	F-W-1.0	90.21	87.50	88.83			
FP-CycleGAN	F-N-0.6	100.00	75.25	85.88	**91.52**	**87.93**	**88.61**
	F-N-0.8	61.07	100.00	75.83			
	F-N-1.0	83.73	87.50	85.57			
	F-Q-0.8	99.43	87.50	93.09			
	F-W-0.6	98.37	90.25	94.13			
	F-W-0.8	100.00	87.50	93.33			
	F-W-1.0	98.04	87.50	92.47			

required to demonstrate that the generated images successfully perform the target defect feature transfer and improve the generalizability of the data.

The specific experimental scheme is:

Construction of a data-free augmented training set: 400 single-angle and 15 multi-angle images for each bearing

defect category except for the label F-N-0.8. The category labelled F-N-0.8 contains 300 plus 400 multi-angle images. In this case, the trained neural network often has low generalization in the test set, because the training lacks data with sufficient generalization. This simulates the problem of often unbalanced data in practical engineering applications, where a small amount of data or a single piece of data often makes it difficult to obtain good detection results.

Construction of the training set after data amplification: each bearing defect category, except for the label F-N-0.8, contains 400 single-angle and 15 multi-angle real images, as well as 896 generated multi-angle dummy images. The category labelled F-N-0.8 contains 300 plus 400 multi-angle real images.

Construction of the test set: Each category in the test set contains 400 images of random rotation speeds and angles to simulate the diversity of data in real applications.

Besides the proposed method FP-CycleGAN, the classical CycleGAN with ResNet block and UNet as backbones and the FP-CycleGAN without D_AB were also used for comparison experiments, thus proving the superiority of the proposed method.

After amplification of the data by different methods, ResNet18 was used uniformly for classification training and the results were compared on the test set, ten times for each training and the average was taken.

Figure 12 shows a comparison of the results of the fake images generated with different data amplification methods. The proposed method outperforms previous algorithms in coping with pattern collapse and maintaining image realism.

Table 5 shows the results of the classification network ResNet18 after different methods of data enhancement. The comparison of the results shows that the accuracy, recall and F1 scores of the classification network trained on the proposed FP-CycleGAN amplified dataset have improved significantly on the test set.

Figure 13 shows the confusion matrix for the classification network trained on the original and different data amplification datasets.

By comparison, the diagnostic accuracy of the classification network trained by all methods is 100% for the bearing images labeled F-N-0.8, but for the other six categories, the proposed method has a great improvement in the accuracy.

V. CONCLUSION

This paper proposes an unsupervised learning framework based on CycleGAN for detecting defects in small sample rolling bearing thermal images. The framework firstly reconstructs the generator for the highly complex rolling bearing defect thermal images to improve the extraction capability of the network for different dimensional features and the reconstruction capability of the images. To avoid the loss of features in the target domain of the generated images, a new D_AB is designed to identify whether the generated image A and the generated image B belong to two different classes, and a new class loss is proposed to ensure that the generated images should keep the fault features of the target domain. Thus, the accurate transfer of fault features is achieved while the non-fault features of the image are highly maintained. In other words, it solves the problem of lack of realism and non-fault features in the generated images, which is often found in adversarial generation networks. Experiments show that the proposed FP-CycleGAN algorithm outperforms the conventional CycleGAN-based feature transfer algorithms in terms of stability and accuracy. It is noteworthy that it provides a new research idea in maintaining the pattern non-collapse and the realism of the generated images while performing feature transfer.

REFERENCES

[1] R. Liu, B. Yang, E. Zio, and X. Chen, "Artificial intelligence for fault diagnosis of rotating machinery: A review," *Mech. Syst. Signal Process.*, vol. 108, pp. 33–47, Aug. 2018, doi: 10.1016/j.ymssp.2018.02.016.

[2] H. Shao, H. Jiang, H. Zhang, and T. Liang, "Electric locomotive bearing fault diagnosis using a novel convolutional deep belief network," *IEEE Trans. Ind. Electron.*, vol. 65, no. 3, pp. 2727–2736, Mar. 2018, doi: 10.1109/TIE.2017.2745473.

[3] J. Xiong, M. Liu, C. Li, J. Cen, Q. Zhang, and Q. Liu, "A bearing fault diagnosis method based on improved mutual dimensionless and deep learning," *IEEE Sensors J.*, vol. 23, no. 16, pp. 18338–18348, Aug. 2023, doi: 10.1109/JSEN.2023.3264870.

[4] S. Yang, X. Gu, Y. Liu, R. Hao, and S. Li, "A general multi-objective optimized wavelet filter and its applications in fault diagnosis of wheelset bearings," *Mech. Syst. Signal Process.*, vol. 145, Nov. 2020, Art. no. 106914, doi: 10.1016/j.ymssp.2020.106914.

[5] F. Dalvand, S. Dalvand, F. Sharafi, and M. Pecht, "Current noise cancellation for bearing fault diagnosis using time shifting," *IEEE Trans. Ind. Electron.*, vol. 64, no. 10, pp. 8138–8147, Oct. 2017, doi: 10.1109/TIE.2017.2694397.

[6] Z. Jia, Z. Liu, C.-M. Vong, and M. Pecht, "A rotating machinery fault diagnosis method based on feature learning of thermal images," *IEEE Access*, vol. 7, pp. 12348–12359, 2019, doi: 10.1109/ACCESS.2019.2893331.

[7] H. Shao, W. Li, M. Xia, Y. Zhang, C. Shen, D. Williams, A. Kennedy, and C. W. de Silva, "Fault diagnosis of a rotor-bearing system under variable rotating speeds using two-stage parameter transfer and infrared thermal images," *IEEE Trans. Instrum. Meas.*, vol. 70, pp. 1–11, 2021, doi: 10.1109/TIM.2021.3111977.

[8] A. Choudhary, T. Mian, and S. Fatima, "Convolutional neural network based bearing fault diagnosis of rotating machine using thermal images," *Measurement*, vol. 176, May 2021, Art. no. 109196, doi: 10.1016/j.measurement.2021.109196.

[9] H. Zhiyi, S. Haidong, Z. Xiang, Y. Yu, and C. Junsheng, "An intelligent fault diagnosis method for rotor-bearing system using small labeled infrared thermal images and enhanced CNN transferred from CAE," *Adv. Eng. Informat.*, vol. 46, Oct. 2020, Art. no. 101150, doi: 10.1016/j.aei.2020.101150.

[10] Y. Liu and K. W. C. Lai, "The performance index of convolutional neural network-based classifiers in class imbalance problem," *Pattern Recognit.*, vol. 137, May 2023, Art. no. 109284, doi: 10.1016/j.patcog.2022.109284.

[11] Z. Ren, T. Lin, K. Feng, Y. Zhu, Z. Liu, and K. Yan, "A systematic review on imbalanced learning methods in intelligent fault diagnosis," *IEEE Trans. Instrum. Meas.*, vol. 72, pp. 1–35, 2023, doi: 10.1109/TIM.2023.3246470.

[12] W. Mao, Y. Liu, L. Ding, and Y. Li, "Imbalanced fault diagnosis of rolling bearing based on generative adversarial network: A comparative study," *IEEE Access*, vol. 7, pp. 9515–9530, 2019, doi: 10.1109/ACCESS.2018.2890693.

[13] X. Yu, H. Yin, L. Sun, F. Dong, K. Yu, K. Feng, Y. Zhang, and W. Yu, "A new cross-domain bearing fault diagnosis framework based on transferable features and manifold embedded discriminative distribution adaption under class imbalance," *IEEE Sensors J.*, vol. 23, no. 7, pp. 7525–7545, Apr. 2023, doi: 10.1109/JSEN.2023.3248950.

[14] W. Zhu, B. Shi, and Z. Feng, "A transfer learning method using high-quality pseudo labels for bearing fault diagnosis," *IEEE Trans. Instrum. Meas.*, vol. 72, pp. 1–11, 2023, doi: 10.1109/TIM.2022.3223146.

[15] X. Ma, Y. Hu, M. Wang, F. Li, and Y. Wang, "Degradation state partition and compound fault diagnosis of rolling bearing based on personalized multilabel learning," *IEEE Trans. Instrum. Meas.*, vol. 70, pp. 1–11, 2021, doi: 10.1109/TIM.2021.3091504.
[16] X. Xia, X. Pan, N. Li, X. He, L. Ma, X. Zhang, and N. Ding, "GAN-based anomaly detection: A review," *Neurocomputing*, vol. 493, pp. 497–535, Jul. 2022, doi: 10.1016/j.neucom.2021.12.093.
[17] D. P. Kingma and M. Welling, "Auto-encoding variational Bayes," 2013, *arXiv:1312.6114*.
[18] I. J. Goodfellow, J. Pouget-Abadie, M. Mirza, B. Xu, D. Warde-Farley, S. Ozair, A. Courville, and Y. Bengio, "Generative adversarial networks," 2014, *arXiv:1406.2661*.
[19] J. Liu, C. Zhang, and X. Jiang, "Imbalanced fault diagnosis of rolling bearing using improved MsR-GAN and feature enhancement-driven CapsNet," *Mech. Syst. Signal Process.*, vol. 168, Apr. 2022, Art. no. 108664, doi: 10.1016/j.ymssp.2021.108664.
[20] M. Mirza and S. Osindero, "Conditional generative adversarial nets," 2014, *arXiv:1411.1784*.
[21] A. Radford, L. Metz, and S. Chintala, "Unsupervised representation learning with deep convolutional generative adversarial networks," 2015, *arXiv:1511.06434*.
[22] M. Arjovsky, S. Chintala, and L. Bottou, "Wasserstein GAN," 2017, *arXiv:1701.07875*.
[23] J.-Y. Zhu, T. Park, P. Isola, and A. A. Efros, "Unpaired image-to-image translation using cycle-consistent adversarial networks," 2017, *arXiv:1703.10593*.
[24] F. Zhou, S. Yang, H. Fujita, D. Chen, and C. Wen, "Deep learning fault diagnosis method based on global optimization GAN for unbalanced data," *Knowl.-Based Syst.*, vol. 187, Jan. 2020, Art. no. 104837, doi: 10.1016/j.knosys.2019.07.008.
[25] J. Chen, G. Yang, H. Khan, H. Zhang, Y. Zhang, S. Zhao, R. Mohiaddin, T. Wong, D. Firmin, and J. Keegan, "JAS-GAN: Generative adversarial network based joint atrium and scar segmentations on unbalanced atrial targets," *IEEE J. Biomed. Health Informat.*, vol. 26, no. 1, pp. 103–114, Jan. 2022, doi: 10.1109/JBHI.2021.3077469.
[26] F. Luleci, F. Necati Catbas, and O. Avci, "CycleGAN for undamaged-to-damaged domain translation for structural health monitoring and damage detection," *Mech. Syst. Signal Process.*, vol. 197, Aug. 2023, Art. no. 110370, doi: 10.1016/j.ymssp.2023.110370.
[27] C. Dong, C. C. Loy, K. He, and X. Tang, "Image super-resolution using deep convolutional networks," *IEEE Trans. Pattern Anal. Mach. Intell.*, vol. 38, no. 2, pp. 295–307, Feb. 2016, doi: 10.1109/TPAMI.2015.2439281.
[28] A. G. Howard, M. Zhu, B. Chen, D. Kalenichenko, W. Wang, T. Weyand, M. Andreetto, and H. Adam, "MobileNets: Efficient convolutional neural networks for mobile vision applications," 2017, *arXiv:1704.04861*.
[29] A. Dosovitskiy, L. Beyer, A. Kolesnikov, D. Weissenborn, X. Zhai, T. Unterthiner, M. Dehghani, M. Minderer, G. Heigold, S. Gelly, J. Uszkoreit, and N. Houlsby, "An image is worth 16 × 16 words: Transformers for image recognition at scale," 2020, *arXiv:2010.11929*.
[30] Z. Liu, Y. Lin, Y. Cao, H. Hu, Y. Wei, Z. Zhang, S. Lin, and B. Guo, "Swin Transformer: Hierarchical vision transformer using shifted windows," 2021, *arXiv:2103.14030*.
[31] Z. Liu, H. Mao, C.-Y. Wu, C. Feichtenhofer, T. Darrell, and S. Xie, "A ConvNet for the 2020s," 2022, *arXiv:2201.03545*.
[32] N. B. Bynagari, "GANs trained by a two time-scale update rule converge to a local Nash equilibrium," *Asian J. Appl. Sci. Eng.*, vol. 8, no. 1, pp. 25–34, Apr. 2019, doi: 10.18034/ajase.v8i1.9.

LUJIALE GUO received the bachelor's degree in mechanical manufacturing and automation from Shijiazhuang Tiedao University, under the supervision of Prof. Xiaohui Gu from the China National Key Laboratory of Traffic Mechanics. He is currently pursuing the Master of Engineering Science degree with the Faculty of Engineering, Universiti Malaya, under the supervision of Prof. Joon Huang Chuah from the Department of Electrical Engineering.

He has been conducting research in the infrared thermal imaging detection of bearings with unbalanced data with the Image Processing (VIP) Laboratory. In the application of machine learning in his previous project, he has mastered various models and skills for CV and NLP, such as CNN, Transformer, GAN, and GNN.

JOON HUANG CHUAH (Senior Member, IEEE) received the B.Eng. degree (Hons.) from Universiti Teknologi Malaysia, the M.Eng. degree from the National University of Singapore, and the M.Phil. and Ph.D. degrees from the University of Cambridge. He is currently a Professor, the President, and the CEO with Southern University College, Malaysia. He is also the Head of the VIP Research Group, Department of Electrical Engineering, Faculty of Engineering, University of Malaya, Malaysia. His research interests include image processing, computational intelligence, IC design, and scanning electron microscopy. He is a fellow and was the Honorary Secretary of the Institution of Engineers, Malaysia (IEM). He was the Honorary Treasurer of the IEEE Computational Intelligence Society (CIS) Malaysia Chapter and the Honorary Secretary of the IEEE Council on RFID Malaysia Chapter. He is the Chairman of the Institution of Engineering and Technology (IET) Malaysia Network. He is a Chartered Engineer registered under the Engineering Council, U.K., and a Professional Engineer registered under the Board of Engineers, Malaysia.

WONG JEE KEEN RAYMOND was born in Perak, Malaysia, in 1987. He received the bachelor's degree in electrical and electronic engineering and the master's degree in electrical engineering from University Tenaga Nasional, Malaysia, in 2010 and 2013, respectively. He is currently pursuing the Ph.D. degree with the University of Malaya, Malaysia. He was a Product Engineer with Motorola Malaysia, from 2010 to 2011. He has been a Research Assistant with the University of Malaya, since 2013. His research interest includes the measurement and classification of partial discharge phenomena in high-voltage power cables.

XIAOHUI GU received the B.S. and Ph.D. degrees in vehicle operation engineering from Shijiazhuang Tiedao University, Shijiazhuang, China, in 2014 and 2018, respectively. He is currently an Associate Professor with the State Key Laboratory of Mechanical Behavior and System Safety of Traffic Engineering Structures, Shijiazhuang Tiedao University. His research interests include vehicle dynamics and fault diagnosis.

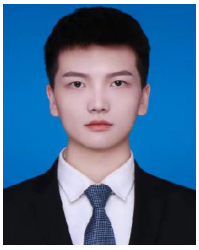

JIE YAO is currently pursuing the master's degree with the Mechanical Engineering School, Shijiazhuang Railway University, under the supervision of Prof. Gu Xiaohui. His research interest includes bearing fault diagnosis.

XIANGQIAN CHANG received the bachelor's degree from the Nanjing University of Science and Technology. His current research interests include deep learning, algorithm optimization, AI4Science, defect detection, and medical image processing.